SUPPORTING INFORMATION FOR

Dual Role of Electron-Accepting Metal-Carboxylate Ligands: Reversible Expansion of Exciton Delocalization and Passivation of Nonradiative Trap-States in Molecule-Like CdSe Nanocrystals

Katie N. Lawrence,[‡] *Poulami Dutta,*[§] *Mulpuri Nagaraju,*[‡] *Meghan B. Teunis,*[‡] *Barry B. Muhoberac,*[‡] *and Rajesh Sardar*[‡,*]

[‡]Department of Chemistry and Chemical Biology, Indiana University-Purdue University Indianapolis, 402 N. Blackford Street, Indianapolis, Indiana 46202, United States

[§]Department of Chemistry, Michigan State University, 578 South Shaw Lane, East Lansing, Michigan 48824, United States

Table S1. HOMO and LUMO levels of Cd(carboxylate)$_2$ complexes calculated in gas phase.

Ligand	Molecular orbital	Energy level (eV) vs. vacuum
Cd(benzoate)$_2$	HOMO	-7.34
	HOMO-1	-7.34
	HOMO-2	-7.41
	LUMO	-1.70
Cd(nonanoate)$_2$	HOMO	-7.86
	HOMO-1	-7.86
	HOMO-2	-8.24
	LUMO	-1.71
Cd(oleate)$_2$	HOMO	-6.67
	HOMO-1	-6.69
	HOMO-2	-7.88
	LUMO	-1.72

The geometries were optimized using the B3LPY method with LANL2DZ basis set for Cd atom and 6-311+G** basis set for C, O, and H atoms.

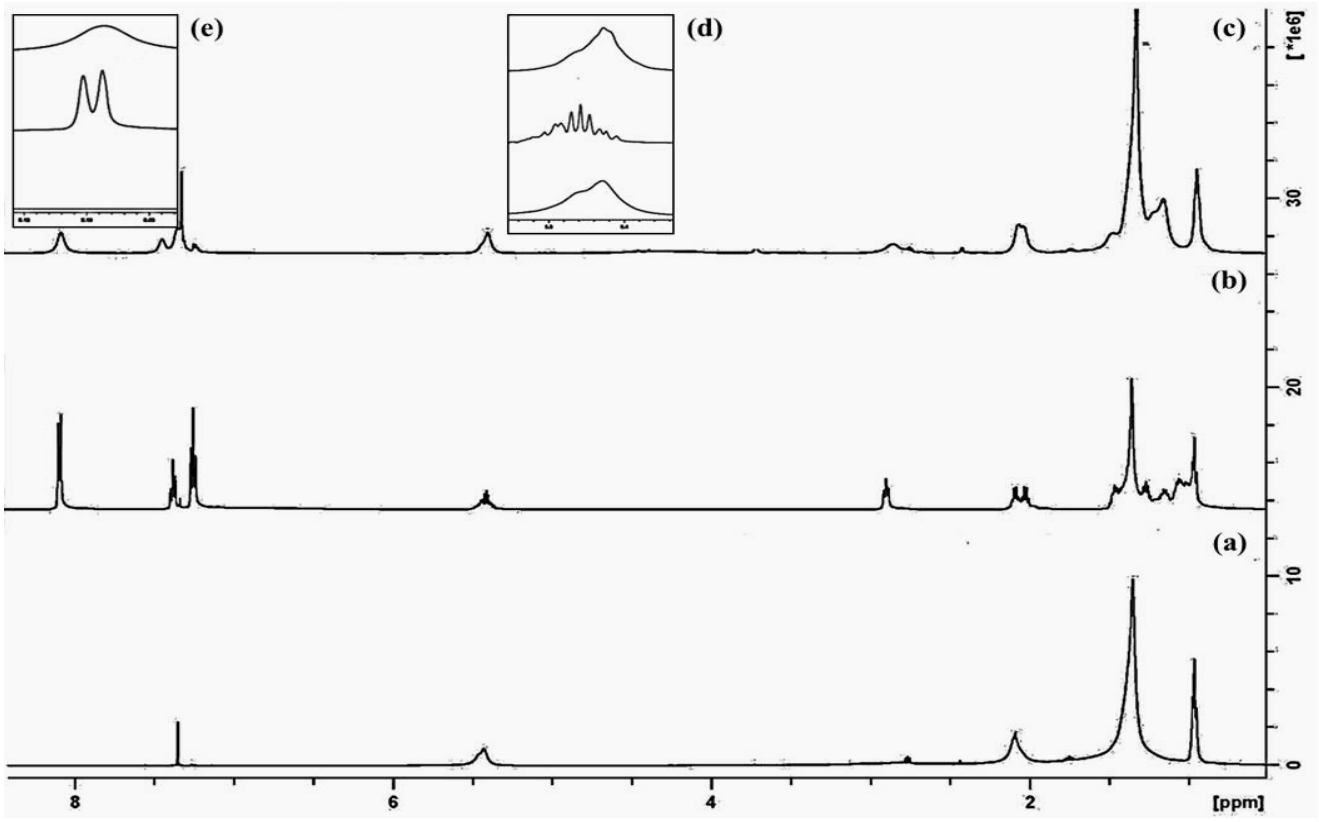

Figure S1. ^{1}H NMR spectra of (a) OLA-passivated $(CdSe)_{34}$ nanocrystals and (c) after $Cd(O_2CPh)_2$ treatment. The spectrum in panel b represents OLA-$Cd(O_2CPh)_2$ complex in the absence of nanocrystals. Inset (d) represents the vinyl resonance of OLA (-CH=CH-) at 5.35 ppm with the top, middle, and bottom scans referring to (a), (b), and (c), respectively. Free OLA (middle) is much sharper than bound OLA (top and bottom). Bound ligands are known to display broader peak signals because of the transversal interproton dipolar relaxation mechanism, which is caused by restricted rotational mobility of ligands attached to the surface, and thus, they tumble more slowly than their free counterparts creating broadening in the spectra.[1-3] Broad peaks at 5.35 and 8.12 ppm from the vinyl resonance of OLA and aromatic resonances of $Cd(O_2CPh)_2$, respectively, suggest that both OLA and $Cd(O_2CPh)_2$ are attached to the surface of the SNC. Inset (e) represents the aromatic resonance (ortho-) of $Cd(O_2CPh)_2$, in which proton signal is much broader for nanocrystal-bound benzoate than OLA-$Cd(O_2CPh)_2$ complex.

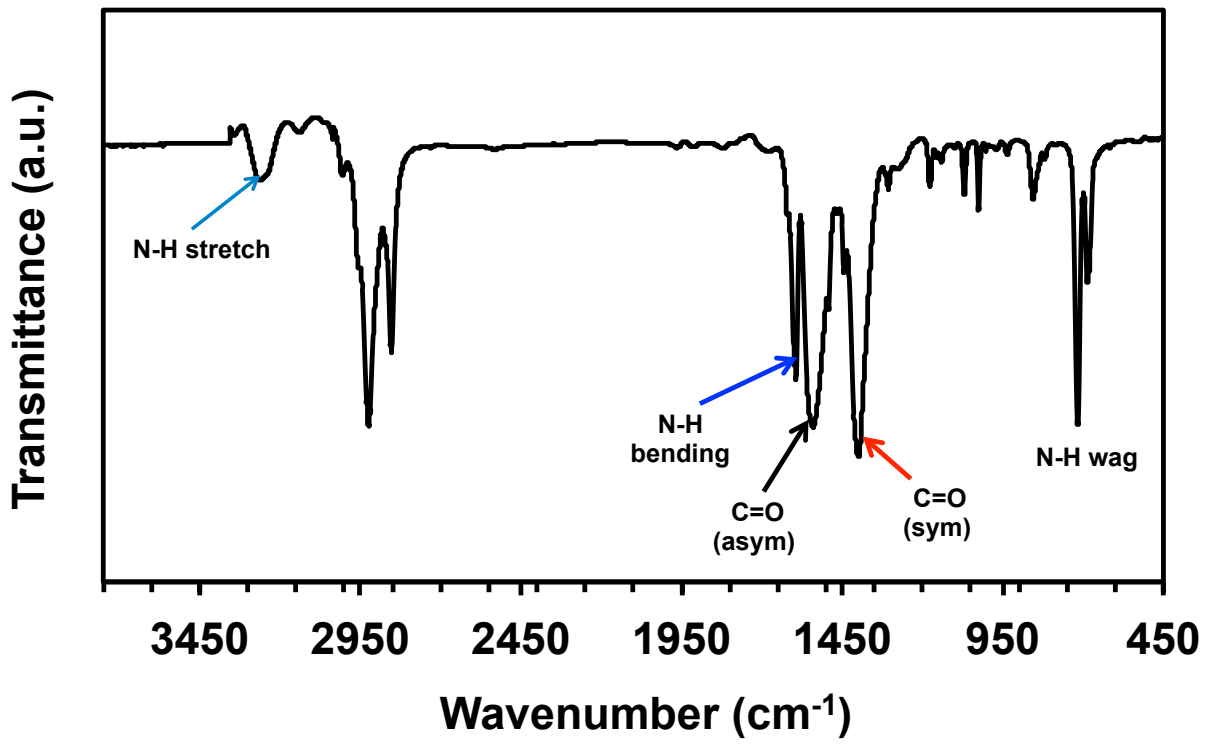

Figure S2. FTIR spectrum of purified OLA-passivated $(CdSe)_{34}$ nanocrystals after binding of $Cd(O_2CPh)_2$. The characteristic N-H stretch in the range of 3400-3300 cm^{-1}, N-H bending mode at 1581 cm^{-1}, and N-H wag at 721 cm^{-1} were present after the addition of $Cd(O_2CPh)_2$, which confirm the attachment of primary OLA to the nanocrystal surface.[4] Additionally, new asymmetric (1518 cm^{-1}) (black arrow) and symmetric (1388 cm^{-1}) (red arrow) stretches of the carboxylate group (C=O) appeared. The separation between these two vibrations is 130 cm^{-1}, suggesting $-COO^-$ attached to the Cd^{2+} through a chelating bidentate interaction. Importantly, presence of both N-H and C=O after the addition of $Cd(O_2CPh)_2$ suggests mixed surface ligation rather than the most commonly observed surface exchange.[2,5]

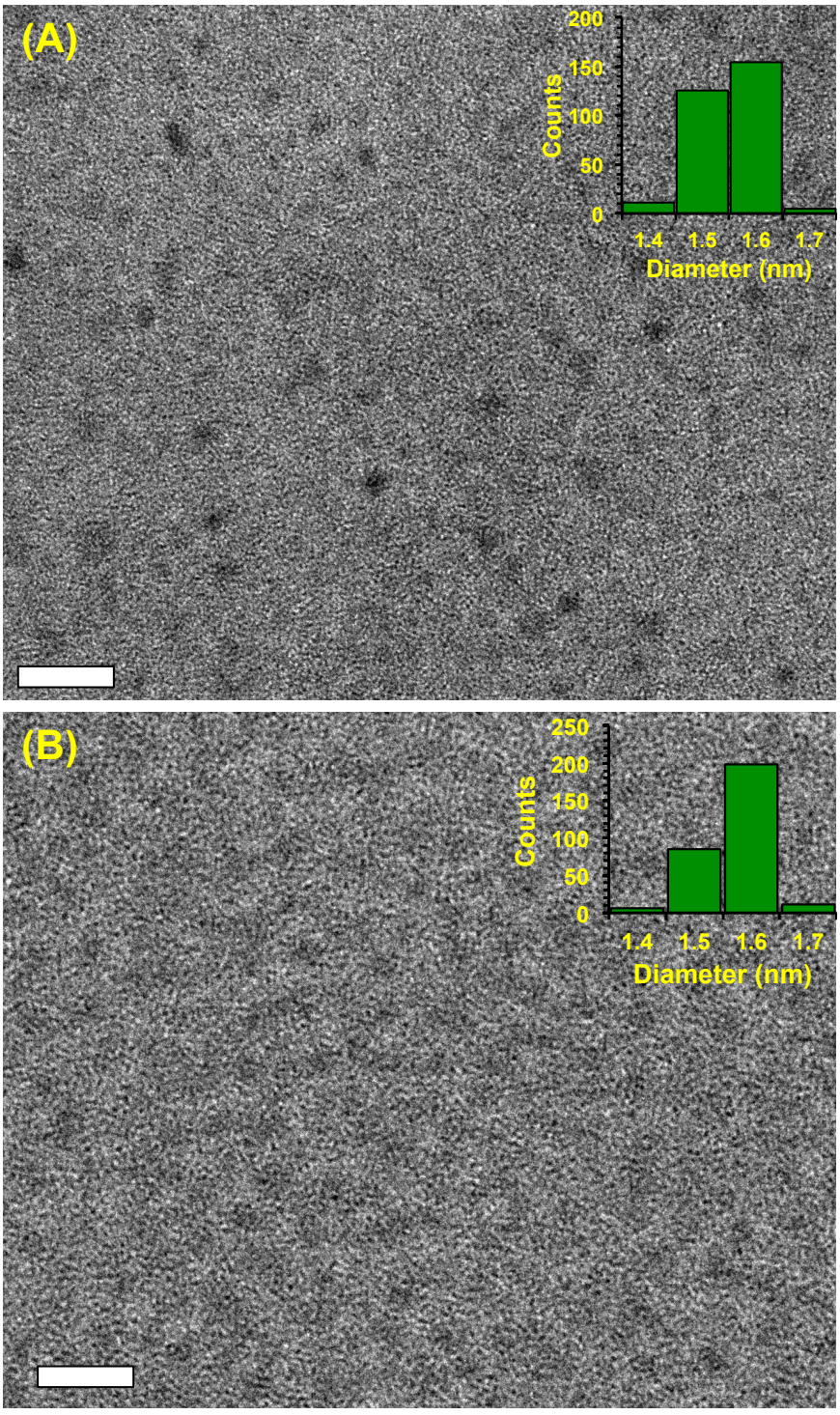

Figure S3. TEM images of OLA-passivated $(CdSe)_{34}$ nanocrystals after synthesis (A) and after binding $Cd(O_2CPh)_2$ (B). The scale bars are 10 nm. The insert shows histogram of nanocrystal size analysis. In each case, 300 nanocrystals were counted to determine the distribution.

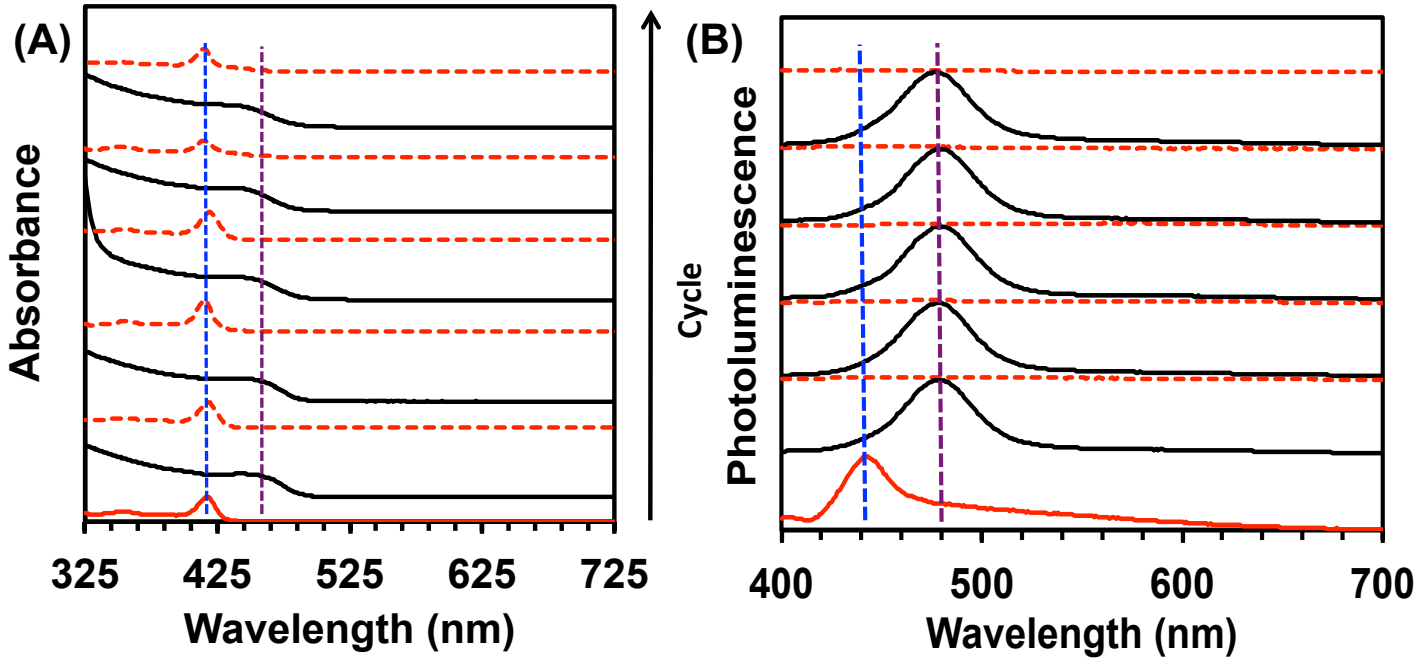

Figure S4. (A) UV-visible absorption and (B) emission spectra (in toluene) of purified OLA-passivated $(CdSe)_{34}$ nanocrystals after synthesis (solid red line), after binding $Cd(O_2CPh)_2$ (solid black lines), and treatment with TMEDA (dotted red lines) at room temperature. The several scans represent cycling between $Cd(O_2CPh)_2$ and TMEDA treatment. The blue and purple dotted lines are markers of the peak position during the reversible exchange of $Cd(O_2CPh)_2$. Due to overlay, the band-edge PL peak position after removal of $Cd(O_2CPh)_2$ by TMEDA is not illustrated.

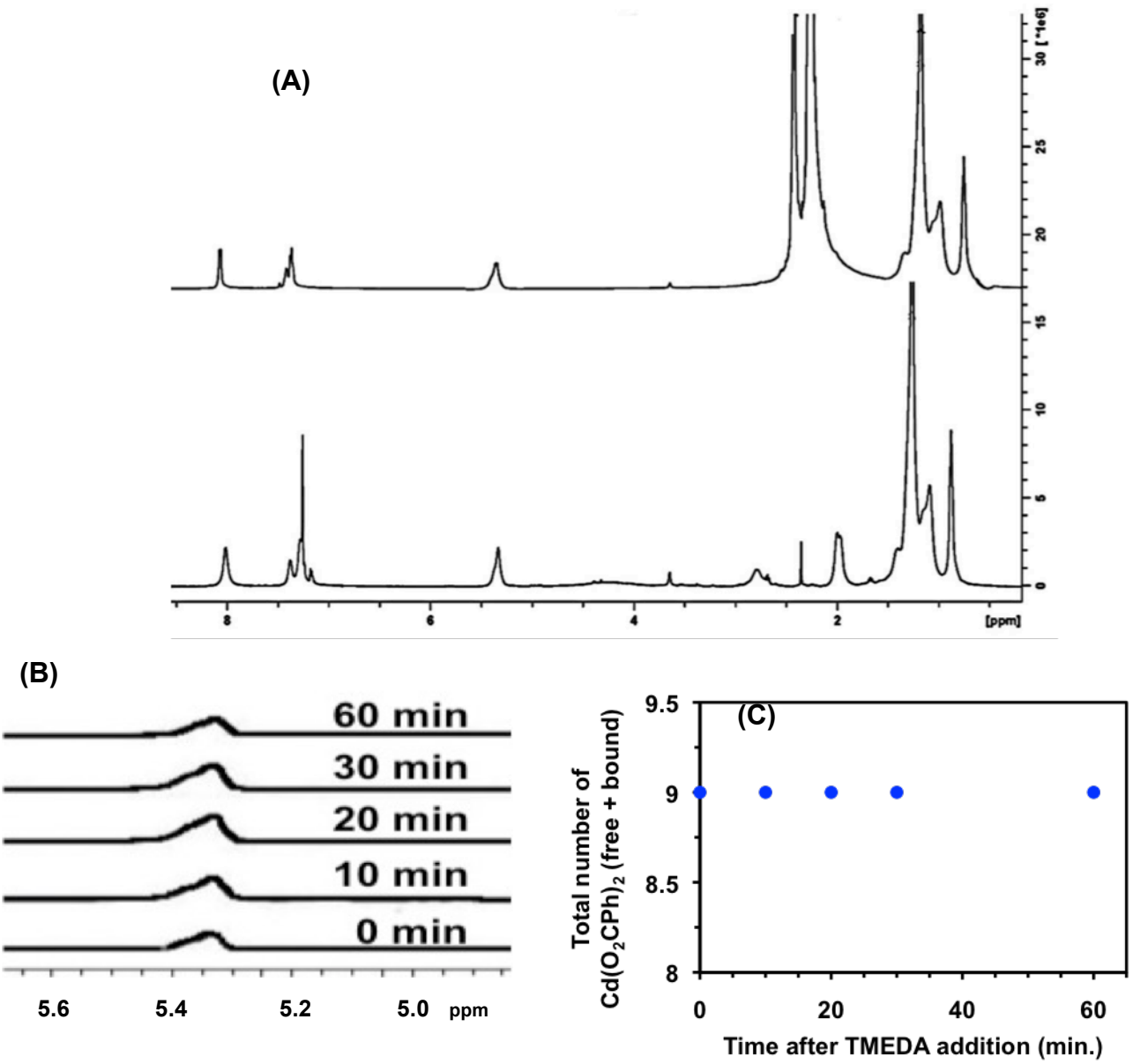

Figure S5. (A) ^{1}H NMR spectra of mixed OLA- and $Cd(O_2CPh)_2$-passivated $(CdSe)_{34}$ nanocrystals (bottom) and after 60 min of TMEDA treatment (top). All spectra were collected in $CDCl_3$. Vinyl resonance (-*CH*=*CH*-) signals at 5.35 from OLA remained broad even after TMEDA treatment, suggested that the OLA is still bound to the surface of the $(CdSe)_{34}$ nanocrystals. (B) The expanded vinyl region of OLA after TMEDA treatment of nanocrystals that had mixed OLA and Cd(O2CPh)2) passivation. (C) Number of bound plus free $Cd(O_2CPh)_2$ per $(CdSe)_{34}$ nanocrystal determined by integrating the phenyl region with respect to vinyl region of OLA assuming each nanocrystal contained 18 OLA ligands. The graph represents a constant number of $Cd(O_2CPh)_2$ present in the solution during TMEDA treatment.

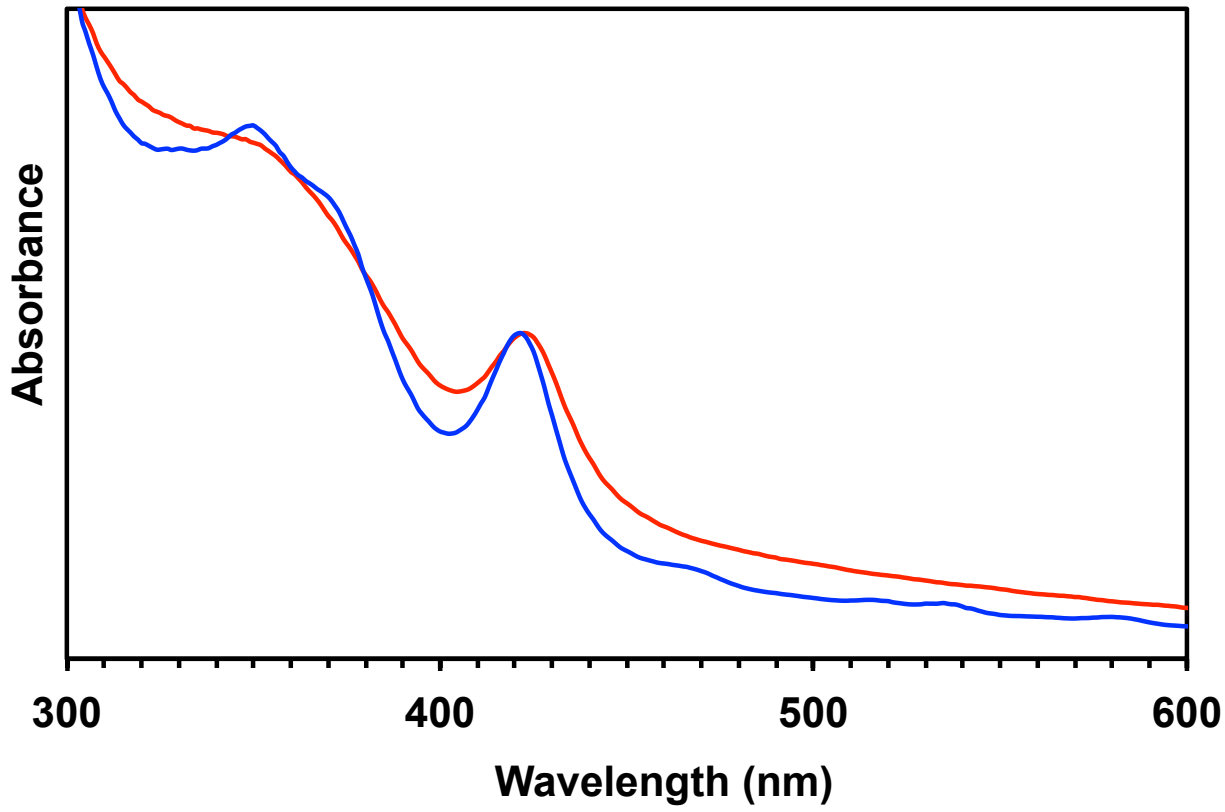

Figure S6. Absorption spectra (in toluene) of purified mixed HDA- and TOP-passivated $(CdSe)_{34}$ nanocrystals (blue line) synthesized according to a literature procedure[6] and after *ex situ* treatment with $Cd(O_2CPh)_2$ (red line) at room temperature. The nanocrystals displayed their lowest energy absorption peak at 415 and 417 nm before and after $Cd(O_2CPh)_2$ treatment, respectively. This ~14 eV shift of the lowest energy absorption peak is minor compared to 260 meV and suggest a minimal contribution of delocalization of exciton wave functions.

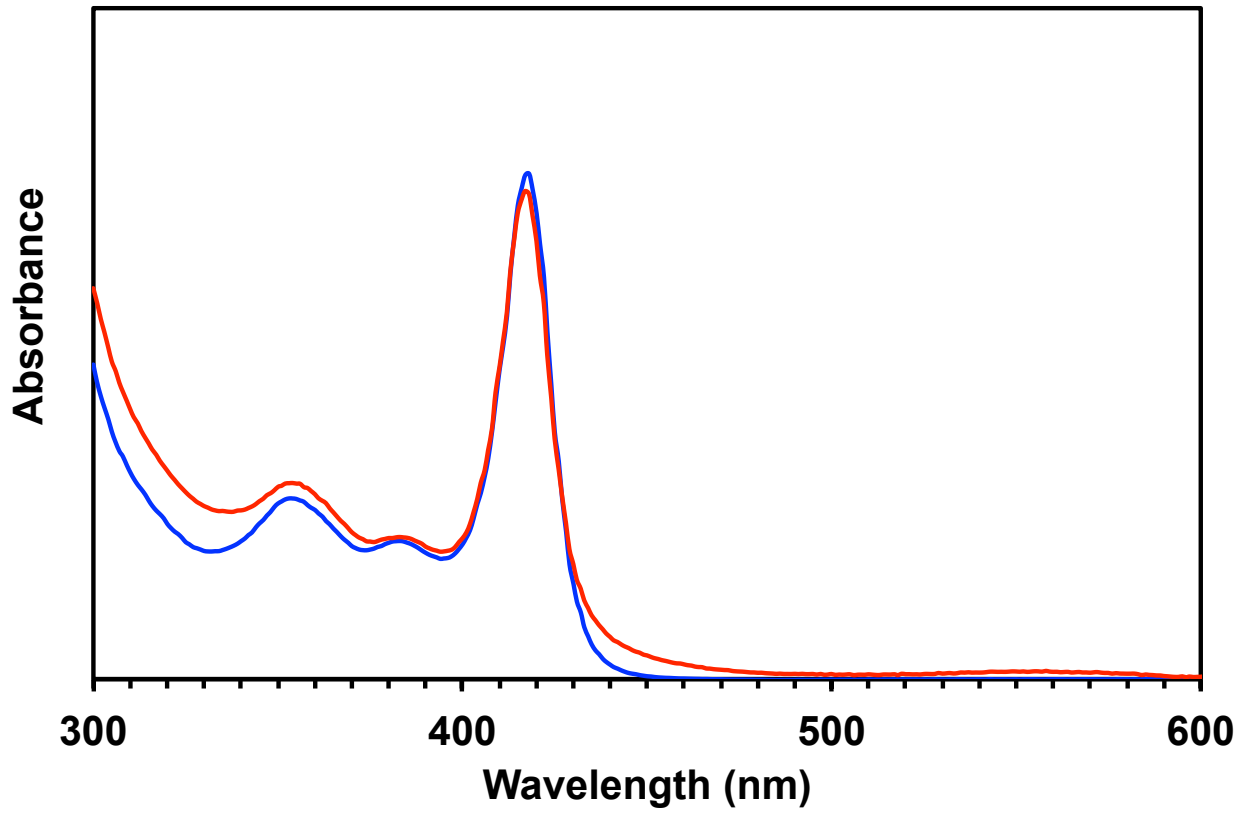

Figure S7. UV-visible absorption spectra (in toluene) of purified OLA-passivated $(CdSe)_{34}$ nanocrystals (blue line) and after *ex situ* treatment with $Cd(nonanoate)_2$ at room temperature (red line).

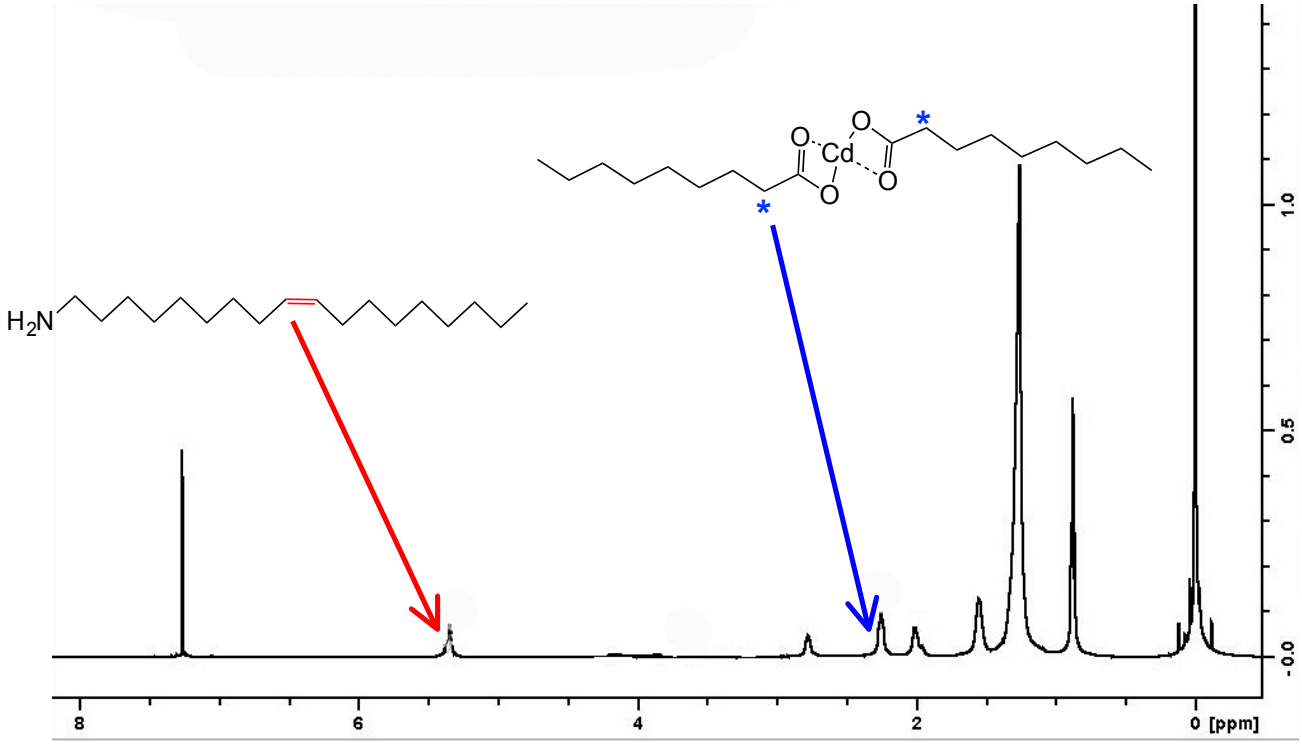

Figure S8. ^{1}H NMR spectra of mixed OLA-passivated $(CdSe)_{34}$ nanocrystals after treatment with Cd(nonanoate)$_2$. The broad vinyl resonance (-CH=CH-) of OLA (5.35 ppm, red arrow) and (CO-CH_2-) proton resonance of Cd(nonanoate)$_2$ (2.38 ppm, blue arrow) suggest mixed nanocrystal surface passivation with a ratio of ~1:1 between (-CH=CH-) and (CO-CH_2-) protons that were observed. Given that $(CdSe)_{34}$ nanocrystals contain a total of 28 surface Cd and Se sites and considering that all Cd sites are occupied by OLA, approximately ~14 Se sites were passivated by Cd(O_2CPh)$_2$. For simplicity bond nanocrystals to these ligands are not shown.

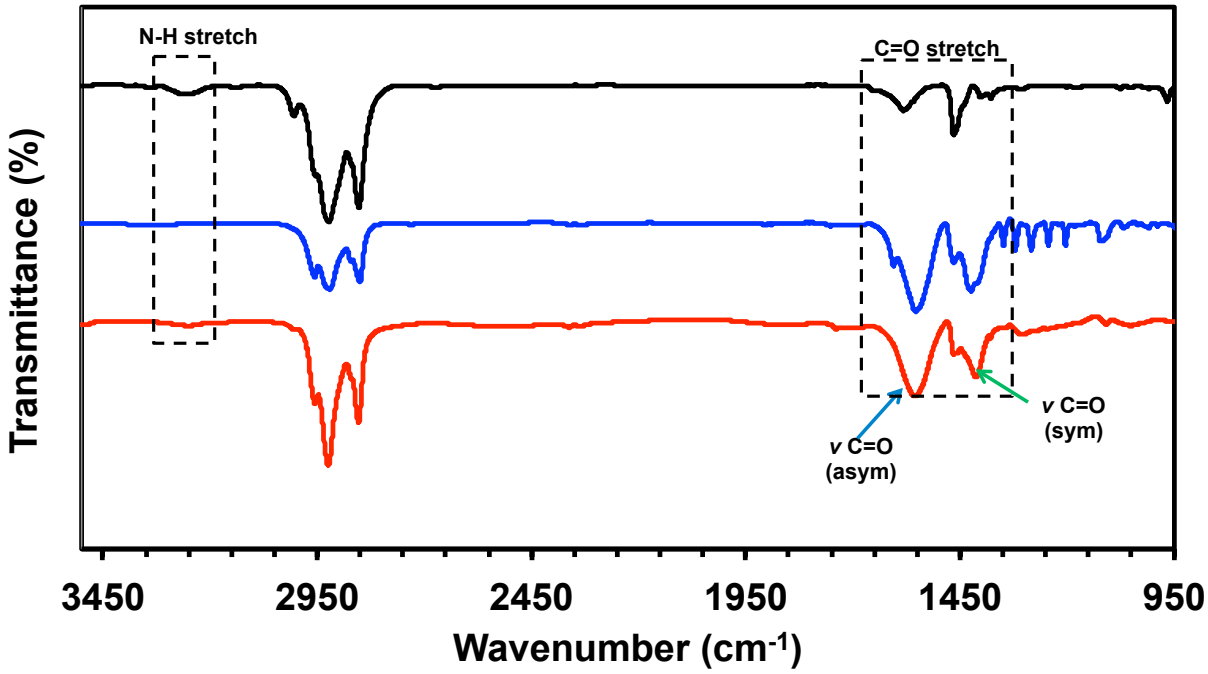

Figure S9. FTIR spectra of OLA-passivated $(CdSe)_{34}$ nanocrystals (black curve) in which characteristic N-H stretch in the range of 3400-3000 cm^{-1} appeared, confirming that the primary amine OLA passivates the nanocrystal surface.[4] After $Cd(nonanoate)_2$ treatment (red curve), new asymmetric (1546 cm^{-1}) and symmetric (1406 cm^{-1}) stretches from the carboxylate group ($-COO^-$) appeared. The separation between these two vibration is 141 cm^{-1}, suggesting $-COO^-$ is attached to the Cd^{2+} through a chelating bidentate interaction.[7-8] Importantly, the asymmetric and symmetric stretches are both red-shifted from 1552 cm^{-1} (~6 cm^{-1}) and 1411 cm^{-1} (~5 cm^{-1}), respectively, along with peak broadening of the pure $Cd(nonanoate)_2$ (blue), which suggests that the interaction between $-COO^-$ and Cd^{2+} is weakened due to Cd^{2+} attached to the surface Se sites. Furthermore, the presence of N-H stretch and N-H bending modes indicate mixed surface ligation, and addition of the Z-type ligand $Cd(nonanoate)_2$ did not replace the L-type ligand OLA, as reported in the literature.[2,5]

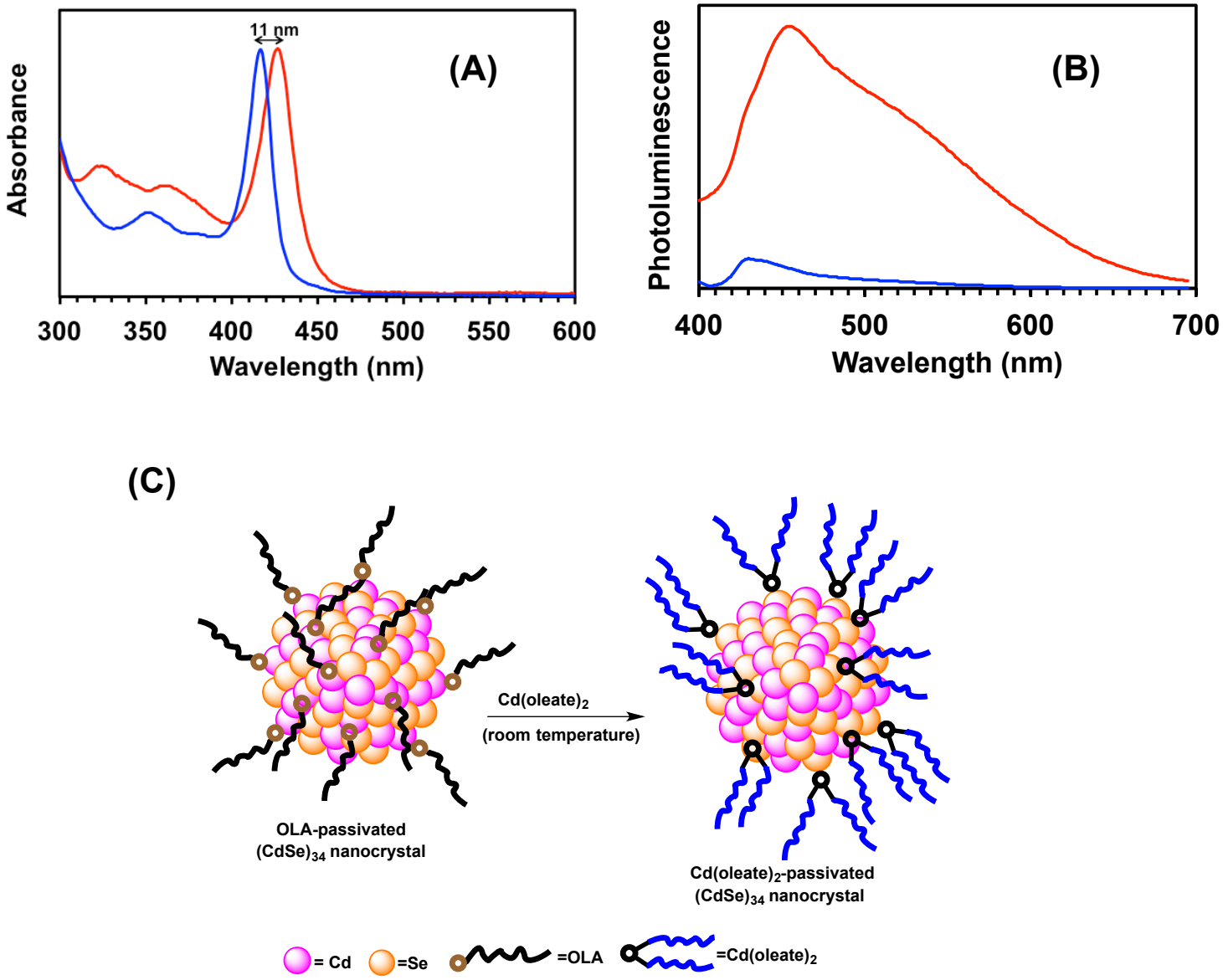

Figure S10. Absorption (A) and emission (B) spectra of purified OLA-passivated $(CdSe)_{34}$ nanocrystals prior to (blue lines) and after (red lines) ex situ treatment with $Cd(oleate)_2$ at room temperature. The emission spectra were collected at 380 nm excitation wavelength. The FWHM of the lowest energy absorption peak changed from 12 nm to 22 nm. The red-shift in the lowest energy absorption peak along with peak broadness after treatment of $Cd(oleate)_2$ indicate the delocalization of hole wave function. As oppose to $Cd(O_2CPh)_2$ treatment in which a substantial increase in the band-edge emission peak (Figure 1B) but not the broad-band emission peak, the treatment of $Cd(oleate)_2$ increased both the peak intensity, which results in a 3.5 fold increased in PLQY. Importantly, appearance of broad emission band covering most of the visible region of the spectrum implies that the surface of the $(CdSe)_{34}$ nanocrystals

was not fully passivated. As illustrated in C, the surface of the original $(CdSe)_{34}$ nanocrystals was passivated with OLA attached to Cd sites keeping Se sites unpassivated that creates nonradiative trap states and broad emission spectra. After treatment of $Cd(oleate)_2$ the surface being passivated with this new ligand, which was attached to the Se sites, keeping the Cd sites unpassivated. This ligand exchange mechanism is in agreement with literature[2,5] but different than $Cd(O_2CPh)_2$ treatment (heterogeneous exchange condition). In the case of $Cd(oleate)_2$ treatment, the ligand exchange was conducted in a homogeneous condition (both OLA-passivated $(CdSe)_{34}$ nanocrystals and $Cd(oleate)_2$ are soluble in toluene). Therefore, presence of large excess of $Cd(oleate)_2$ in the exchange medium could result in the formation of OLA-$Cd(oleate)_2$ complex and release in the reaction medium, as reported by Owen and coworkers.[2] Our hypothesis concerning surface ligand chemistry is further supported by FTIR analysis as discussed in Figure S12.

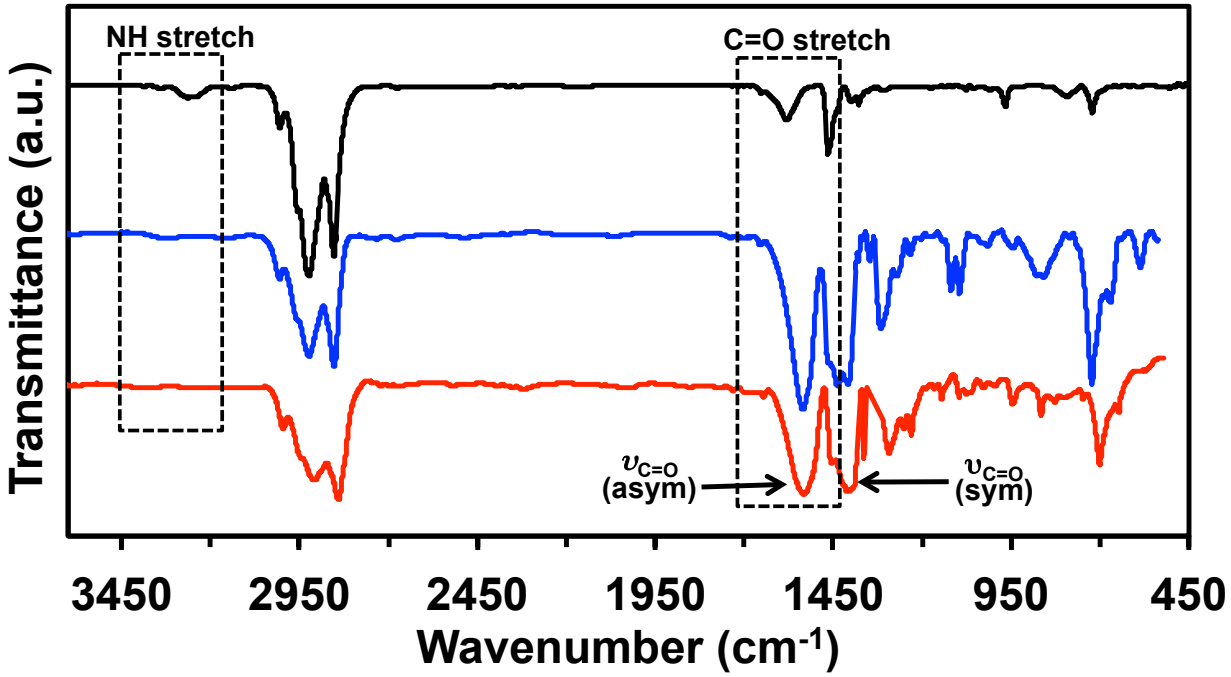

Figure S11. FTIR spectra of OLA-passivated $(CdSe)_{34}$ nanocrystals (black), pure $Cd(oleate)_2$ (blue), OLA-passivated $(CdSe)_{34}$ nanocrystals after addition of $Cd(oleate)_2$ (red). Broad N-H stretch mode is present at ~3250 cm^{-1} for OLA-passivated $(CdSe)_{34}$ nanocrystals which disappeared after addition of $Cd(oleate)_2$ to $(CdSe)_{34}$ nanocrystals (red). Upon addition of $Cd(oleate)_2$ new asymmetric (1531 cm^{-1}) and symmetric (1396 cm^{-1}) stretching vibrations of the carboxylate group ($-COO^-$) replaced the original amine peaks suggesting a ligand exchange. The separation between the two observed stretching vibrations (135 cm^{-1}) is indicative of chelating bidentate interaction.[7-8] Most importantly, both the asymmetric and symmetric vibration red-shifted from 1535 (~4 cm^-

^{1}, 18 nm) and 1406 cm^{-1} (~10 cm^{-1}, 51 nm), respectively, along with peak broadening of the pure $Cd(oleate)_2$ (purple), suggesting the interaction between $-COO^{-}$ and Cd^{2+}weakened due to their attachment to the nanocrystal surface.

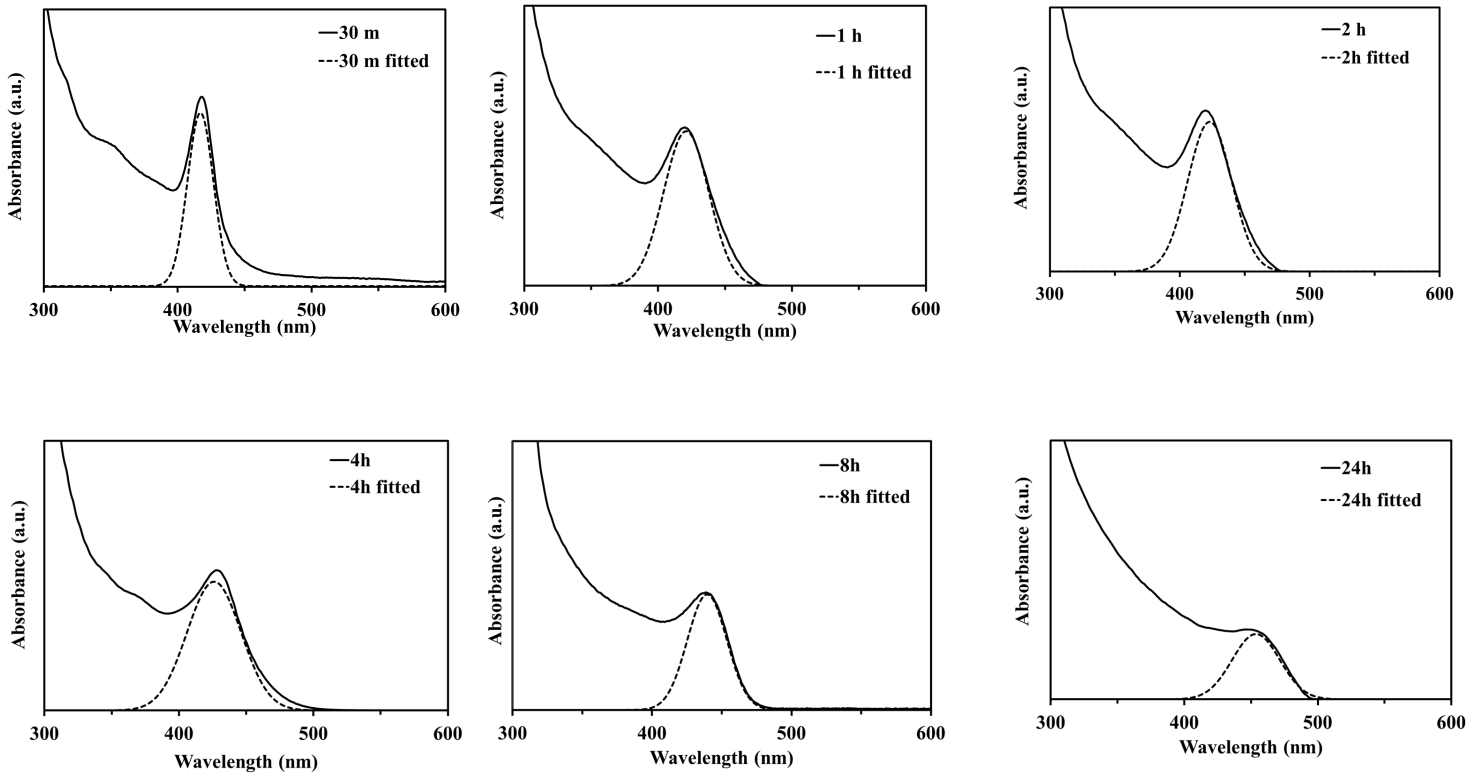

Figure S12. Time-dependent ground-state absorption spectra (solid lines) of OLA-passivated $(CdSe)_{34}$ nanocrystals after treatment of $Cd(O_2CPh)_2$ at room temperature. Origin 6.0 software was used to fit the absorption peak (dotted lines) in order to determine the exact wavelength value, which was further used to calculate the arrarent increase in the excitonic radius (delocalization radius, ΔR) of the $(CdSe)_{34}$ nanocrystals using an empirical formula.[9]

Table S2. Comparison of emission properties of $(CdSe)_{34}$ nanocrystals passivated with different types of ligands.

surface passivating ligand	quantum yield (%) (PLQY)	PL lifetime (τ) (ns)	radiative rate constant (k_r) (s^{-1})	radiative lifetime (τ_r) (s)	nonradiative rate constant (k_{nr}) (s^{-1})
OLA	5 ± 0.7	13.7 ± 2.0	3.7×10^6	2.7×10^{-7}	69.5×10^6
Mixed OLA and $Cd(benzoate)_2$	70 ± 3	45.5 ± 6.9	15.6×10^6	6.4×10^{-8}	6.4×10^6
Mixed OLA and $Cd(nonanoate)_2$	46 ± 6	39.1 ± 4.5	11.8×10^6	8.5×10^{-8}	13.8×10^6
$Cd(oleate)_2$	18 ± 4	17.4 ± 2.3	10.3×10^6	9.7×10^{-8}	47.2×10^6

Quantum yield of coumarin-30 in acetonitrile is 55.3% at 380 nm excitation[10] was used to determine the percentage PLQY of various ligand-passivated $(CdSe)_{34}$ nanocrystals. Stretch exponential equation[11] was employed to determine the radiative lifetime. PL lifetime (τ) = $1/(k_r + k_{nr})$, PLQY = $k_r/(k_r + k_{nr})$, radiative lifetime (τ_r) = $1/k_r$.[12]

REFERENCES

(1) Hens, Z.; Martins, J. C. *Chem. Mater.* **2013**, *25*, 1211-1221.

(2) Anderson, N. C.; Hendricks, M. P.; Choi, J. J.; Owen, J. S. *J. Am. Chem. Soc.* **2013**, *135*, 18536-18548.

(3) Badia, A.; Demers, L.; Dickinson, L.; Morin, F. G.; Lennox, R. B.; Reven, L. *J. Am. Chem. Soc.* **1997**, *119*, 11104-11105.

(4) Cooper, J. K.; Franco, A. M.; Gul, S.; Corrado, C.; Zhang, J. Z. *Langmuir* **2011**, *27*, 8486-8493.

(5) Zhou, Y.; Wang, F.; Buhro, W. E. *J. Am. Chem. Soc.* **2015**, *137*, 15198-15208.

(6) Kuçur, E.; Ziegler, J.; Nann, T. *Small* **2008**, *4*, 883-887.

(7) Cossairt, B. M.; Owen, J. S. *Chem. Mater.* **2011**, *23*, 3114-3119.

(8) Chen, O.; Yang, Y.; Wang, T.; Wu, H.; Niu, C.; Yang, J.; Cao, Y. C. *J. Am. Chem. Soc.* **2011**, *133*, 17504-17512.

(9) Yu, W. W.; Qu, L.; Guo, W.; Peng, X. *Chem. Mater.* **2003**, *15*, 2854-2860.

(10) Senthilkumar, S.; Nath, S.; Pal, H. *Photochem. Photobiol.* **2004**, *80*, 104-111.

(11) Shi, D.; Adinolfi, V.; Comin, R.; Yuan, M.; Alarousu, E.; Buin, A.; Chen, Y.; Hoogland, S.; Rothenberger, A.; Katsiev, K.; Losovyj, Y.; Zhang, X.; Dowben, P. A.; Mohammed, O. F.; Sargent, E. H.; Bakr, O. M. *Science* **2015**, *347*, 519-522.

(12) Park, Y.-S.; Bae, W. K.; Pietryga, J. M.; Klimov, V. I. *ACS Nano* **2014**, *8*, 7288-7296.